

# The Casimir Effect for Arbitrary Optically Anisotropic Materials

José C. Torres-Guzmán<sup>1,2,\*</sup> and W. Luis Mochán<sup>1,†</sup>

<sup>1</sup>*Instituto de Ciencias Físicas, Universidad Nacional Autónoma de México,  
Apdo. Postal 48-3, 62251 Cuernavaca, Morelos, México*

<sup>2</sup>*Facultad de Ciencias, Universidad Autónoma del Estado de Morelos,  
Avenida Universidad 1001, 62221 Cuernavaca, Morelos, México*

(Dated: May 17, 2022)

We extend a fictitious-cavity approach to calculate the Casimir effect for cavities bounded by flat anisotropic materials. We calculate the energy, force and torque in terms only of the optical coefficients of the walls of the cavity. We calculate the Casimir effect at zero and finite temperature for some simple systems. As a non trivial application, we calculate the torque between a semi-infinite anisotropic plate and an anisotropic film. We study the effect of the film thickness in the torque and find an optimal width that maximizes the torque.

PACS numbers: 42.50.Pq 31.30.jh 42.50.Lc 12.20.Ds

## I. INTRODUCTION

An electromagnetic mode of frequency  $\omega$  within an electromagnetic cavity is analogous to a harmonic oscillator with a quantized energy spectrum given by semi-integer multiples  $n + 1/2$  of the energy quantum  $\hbar\omega$ , where the integer  $n$  is the occupation number of the mode, i.e., the number of photons in the corresponding state,  $\hbar\omega$  is the quantized energy of each photon and  $\hbar\omega/2$  is the ground state energy arising from the quantum nature of the electromagnetic field and its *zero point fluctuations*. As the frequency of the electromagnetic modes depends on the geometry of the cavity, the zero point fluctuations may not be simply disregarded as a constant contribution to the energy and should be accounted for in calculations of the total energy of the system. A simple vacuum cavity may be produced by positioning two flat conducting plates parallel to each other a small distance  $L$  apart, leading to a first quantization of the electromagnetic field within the cavity. In 1948, Casimir [1] predicted that the vacuum electromagnetic energy due to the quantum fluctuations of the field would depend on  $L$  and therefore a force, which turns out to be attractive, would act on each plate. This Casimir force also may be conceived as originated from the difference between the radiation pressure due to the fluctuating electromagnetic modes outside the plates and the modes within [2]. Irrespective of its interpretation, the Casimir force has its origin in the linear momentum carried by the radiation field. Nevertheless, the radiation field carries angular momentum beyond linear momentum. Therefore, if the plates are optically anisotropic, a Casimir torque might develop besides the Casimir force. In fact, the transfer of angular momentum of polarized light to a macroscopic birefringent medium, resulting in a torque, has been known for a long time [3]. The Casimir torque may be interpreted as arising from the orientational dependence of the vacuum electromagnetic energy, specifically from the dependence on the relative orientation of the optical axes of the plates. The resultant torque tends to align the optical axes along the configuration that minimizes the vacuum energy.

Recently, the Casimir effect has received considerable attention for its possible technological applications, besides the fact that experimental studies have attained the necessary accuracy to test in detail the theoretical predictions [4–17]. Therefore, theories about the Casimir effect that account realistically for the properties of actual materials have become indispensable. The study of vacuum forces between real materials was pioneered by Lifshitz [18], who considered two semi-infinite homogeneous and isotropic non-spatially dispersive dielectric slabs, whose fluctuating currents were the sources of the fluctuating electromagnetic field and whose correlations were related to the dielectric response of the materials.

In 1972, Parsegian and Weiss derived an expression in the non-retarded limit for the interaction energy between two semi-infinite dissipationless dielectric anisotropic materials [19] following a method of surface mode summation. Barash derived an expression which included retardation and dissipation effects [20] employing an auxiliary system [21] first introduced for isotropic systems. The solutions of Maxwell's equations for the field in inhomogeneous and absorbing media were expanded in terms of the orthogonal solutions of Maxwell's equations for a non-dissipative auxiliary system in which the frequency dependence of the dielectric function is only parametric.

---

\*Electronic address: torres@fis.unam.mx

†Electronic address: mochan@fis.unam.mx

The use of an auxiliary system was further developed in physical terms by Kupiszewska [22] in a calculation of Casimir forces for lossy and dispersive isotropic dielectrics in the case of one dimensional propagation of electromagnetic waves. The problem of quantizing a dissipative system is attacked by accounting both for the dynamics of the vacuum modes and of the atomic dipoles to which they couple and which make up the material, together with a thermal reservoir in which the atomic radiators dissipate the absorbed energy. That formalism was extended by van Enk [23] to obtain the torque between anisotropic materials in the 1D case. In his work, van Enk calculated the torque starting from the flux of the spin angular momentum of the electromagnetic field.

Numerical calculations have also been performed for materials with a small anisotropy using Barash's results and it has been shown that the torque may be large enough to be experimentally measurable in several novel experimental configurations [24]. By a similar technique, the Casimir energy between anisotropic dielectric plates [25], and between a plate with anisotropic magnetic response and another with anisotropic dielectric response [26] have been calculated and analytical approximate expressions for the torque and force were obtained in the retarded limit. Kenneth and Nussinov have also calculated the Casimir energy between parallel plates made up of arrays of wires aligned along different directions [27] using a path integral technique [28, 29].

In the works described above, specific models of the dielectric properties of the plates were assumed from the onset in order to derive expressions for the Casimir force and torque. However, recent works [30–36] have shown that if the theory is set up in terms of the reflection coefficients of the media, or equivalently, in terms of their exact surface impedance [37, 38], it is possible to decouple the calculation of the Casimir force from the calculation of the dielectric response of the materials.

Lambrecht *et al.* have extended their scattering approach [30, 31] to corrugated systems [39]. Moreover, they have argued that the resulting formula for the Casimir energy has a wider range of applicability and may be used to study other anisotropic mirrors. Their formula has been used to evaluate numerically the effects of corrugation on the Casimir force [40] and torque [41] and to calculate the Casimir force between anisotropic metamaterials [42].

Mochán *et al.* [32–36] have argued that in thermal equilibrium, all of the properties of the radiation field within a cavity are completely determined by the optical reflection amplitudes of the walls. Indeed, whenever a photon reaches the surface of a wall of the cavity it may be coherently reflected with an amplitude described by the optical coefficients of the wall. Otherwise, it would be transmitted into the wall to be either absorbed, exciting the material degrees of freedom of its constituents, or transmitted across the wall and into the surrounding vacuum to be lost forever. The probability of these processes is again determined by the optical coefficients of the wall, and given by their squared modulus. In thermodynamic equilibrium, detailed balance implies that whenever a photon is lost, an equivalent photon is incoherently injected back to the cavity, so that both, the coherently and incoherently reflected photons are determined by the reflection amplitudes alone. Therefore, the radiation field within a real cavity would be identical to the field within any cavity that has walls with the same optical properties. This fact allowed the construction of fictitious dissipationless systems which can be simply treated quantum mechanically to obtain the vacuum energy and force for cavities with arbitrary walls. Thus, expressions for the Casimir force obtained from the electromagnetic stress tensor can be applied to semi-infinite or finite, homogeneous or layered, local or spatially dispersive, transparent or opaque systems through a simple substitution of the appropriate optical coefficients. This formalism has allowed the calculation of the Casimir force between photonic structures [43], non-local excitonic semiconductors [44], non-local-plasmon-supporting metals with sharp boundaries [32–36, 45], and between realistic spatially dispersive metals with a smooth self-consistent electronic density profile [46]. With a few modifications, it has also been employed for the calculation of other macroscopic forces, such as those due to electronic tunneling across an insulating gap separating two conductors [47].

The relative simplicity of the formalism developed in [32–36] has allowed its generalization to anisotropic systems [48]. In Ref. [48] a new derivation of the Casimir torque within 1D cavities with walls made up of arbitrary materials characterized only by their anisotropic optical coefficients was presented. By 1D cavity we mean one in which the field is constrained to propagate only along one direction, namely, the normal to the surface of the cavity walls. In the present paper we generalize this formalism to 3D cavities with anisotropic walls. We calculate the Casimir force from the electromagnetic stress tensor. A simple integration over the separation distance  $L$  yields then the vacuum energy. The torque is then calculated by taking the derivative respect to the angle  $\gamma$  between the optical axes of the plates. As our formalism is based on the calculation of the force, which is a directly observable quantity, it avoids the cumbersome singularities that plague other approaches. Furthermore, our results are written directly in terms of the optical coefficients of the walls of the cavity about which we make no assumption. Thus, they can be applied immediately to manifold systems such as insulating or conducting anisotropic slabs either dissipationless or dissipative, to semiinfinite or finite walls and to homogeneous or structured materials. We test the validity of our approach by reproducing some known results [24, 25, 27, 30–36, 42] and we show its versatility by applying it to some previously unexplored systems.

The structure of the paper is the following: In section II we develop our formalism in order to arrive at expressions for the Casimir energy between arbitrary anisotropic plates. The use of an effective cavity allows our results to be

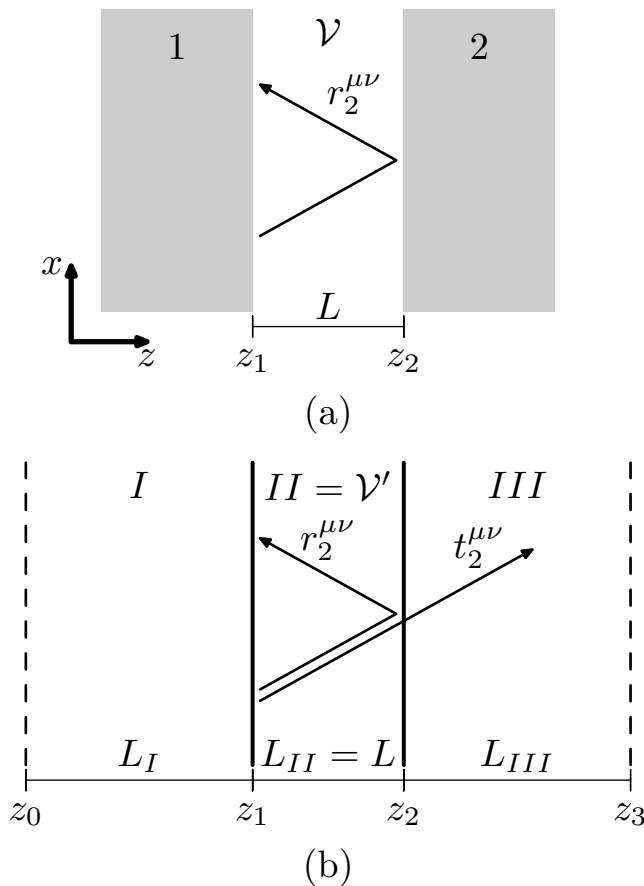


FIG. 1: (a) Vacuum cavity  $\mathcal{V}$  of width  $L$  bounded by two arbitrary anisotropic material slabs (1 and 2) with surfaces at  $z_1$  and  $z_2$  and anisotropic reflection amplitudes  $r_a^{\mu\nu}$  ( $a = 1, 2$ ,  $\mu, \nu = s, p$ ). (b) Fictitious system made up three empty regions  $I$ ,  $II$ , and  $III$ , bounded by perfect mirrors at  $z_0$  and  $z_3$  and with infinitely thin sheets at  $z_1$  and  $z_2$  with identical reflection amplitudes  $r_a^{\mu\nu}$  to those of the real system and corresponding transmission amplitudes  $t_a^{\mu\nu}$ .

applicable to arbitrary slabs at any temperature  $T$ . In section III we specialize our results to semi-infinite local uniaxial media and we apply our results to a calculation of the energy and torque for an idealized uniaxial system consisting of anisotropic mirrors that are perfectly conducting along one direction and perfectly insulating along the perpendicular directions. These calculations are performed for temperatures  $T = 0$  and  $T \neq 0$ . We also consider systems with a finite frequency-dependent conductivity along the optical axis. As a further application of our formalism, in section IV we calculate the torque of a system consisting of two conducting plates with an anisotropic effective mass tensor, where one of the plates is a film with finite thickness  $d$ , and we find there is an optimum value of  $d$  that maximizes the torque. We also calculated the same system considered by Munday et al. [24] consisting of a semi-infinite slab of  $\text{BaTiO}_3$  and a thin film of calcite. Finally, in section V we present our conclusions.

## II. THE EFFECTIVE CAVITY APPROACH

Consider the setup shown in Fig. 1(a). The slabs represents arbitrary media. According to [32–36, 48, 49], in thermodynamic equilibrium the properties of the radiation field within the cavity  $\mathcal{V}$  are completely determined by the geometry of the cavity, characterized by  $L$ , and by the  $2 \times 2$  reflection amplitude matrices  $r_a^{\mu\nu}$  of each slab ( $a = 1, 2$ ) coupling  $\nu$ -polarized incident light to  $\mu$ -polarized reflected light ( $\mu, \nu = s, p$ ). Any relevant property of the material is completely accounted for through its optical coefficients. Thus, the electromagnetic radiation within the real cavity  $\mathcal{V}$  must be identical to that within a fictitious cavity  $\mathcal{V}' = II$  bounded by infinitely thin sheets at  $z_1$  and  $z_2$ , provided their reflection amplitudes  $r_a^{\mu\nu}$  are chosen to match those of the walls of the real cavity  $\mathcal{V}$ . The transmission amplitudes  $t_a^{\mu\nu}$  of the infinitely thin sheets are conveniently chosen in order to guarantee energy conservation with no absorption whatsoever of electromagnetic energy. Thus, there is no absorption in the fictitious system, there is no excitation of material degrees of freedom and the normal modes of its electromagnetic field form a complete orthogonal basis of the

corresponding Hilbert space. As a consequence, one is allowed to use well developed quantum-mechanical procedures for the calculation of the field properties without the requirement of a microscopic model of the material.

The field modes may be quantized and counted by choosing suitable boundary conditions. For example, we can add perfect mirrors far away from the walls of the real cavity (Fig. 1(b)), at  $z_0$  and  $z_3$ . These quantizing mirrors produce a field that mimics the incoherent radiation back into the cavity that is responsible for maintaining a detailed balance and thus the thermodynamic equilibrium.

Consider now a single wave of frequency  $\omega$  with wave-vector projection  $\vec{Q}$  along the interface. Without loss of generality, we choose  $x - z$  as the plane of incidence, so the electric and magnetic fields are given by

$$\vec{E}(\vec{r}, t) = \mathcal{E}_0 e^{i(Qx - \omega t)} \left[ \phi^s(z) \hat{\mathbf{y}} - \frac{1}{iq} (iQ\hat{\mathbf{z}} - \hat{\mathbf{x}}\partial_z) \phi^p(z) \right] \quad (1)$$

and

$$\vec{B}(\vec{r}, t) = \mathcal{E}_0 e^{i(Qx - \omega t)} \left[ \phi^p(z) \hat{\mathbf{y}} + \frac{1}{iq} (iQ\hat{\mathbf{z}} - \hat{\mathbf{x}}\partial_z) \phi^s(z) \right], \quad (2)$$

where  $q = \omega/c$  is the free-space wavenumber,  $\phi^p(z)$  and  $\phi^s(z)$  are the  $p$  and  $s$  polarized components of a spinorial normalized *wave-function*

$$\phi^\mu(z) = C_\Lambda^{\mu r} e^{ikz} + C_\Lambda^{\mu l} e^{-ikz}, \quad (3)$$

where  $C_\Lambda^{\mu\zeta}$  are constant coefficients within each region  $\Lambda = I, II, III$  corresponding to  $\mu$ -polarized light moving towards the right ( $\zeta = r$ ) and left ( $\zeta = l$ ), and  $k = \sqrt{(\omega^2/c^2 - Q^2)}$  is the wave-vector component perpendicular to the interface.

We integrate the energy density,

$$u = (|E|^2 + |B|^2)/16\pi \quad (4)$$

to obtain the total electromagnetic energy

$$\mathcal{U} = \frac{A|\mathcal{E}_0|^2}{8\pi} (L_I \|C_I\|^2 + L_{III} \|C_{III}\|^2), \quad (5)$$

in the limit  $L_I, L_{III} \rightarrow \infty$ , where  $A$  is the area of the plates and  $\|C_\Lambda\|^2 \equiv \sum_{\mu\zeta} |C_\Lambda^{\mu\zeta}|^2$ . In the same limit the normalization condition imposed on the wave-function simplifies to

$$1 = (L_I \|C_I\|^2 + L_{III} \|C_{III}\|^2). \quad (6)$$

Notice that most of the energy lies in the large fictitious regions I and III, so we may identify

$$\mathcal{U} = \frac{A|\mathcal{E}_0|^2}{8\pi} \quad (7)$$

and solve for the amplitude  $|\mathcal{E}_0|^2 = 8\pi\mathcal{U}/A$ . To obtain the force on the slab 2, we calculate the stress tensor  $T_{ij} = (1/8\pi)\text{Re}[E_i E_j^* + B_i B_j^* - (|E|^2 + |B|^2)\delta_{ij}/2]$  at an arbitrary position  $z$  within the cavity,

$$-T_{zz}(z) = \frac{\mathcal{U}}{2Aq^2} \left( k^2 (|\phi^s|^2 + |\phi^p|^2) + |\partial_z \phi^s|^2 + |\partial_z \phi^p|^2 \right). \quad (8)$$

By applying boundary conditions at  $z_0$  and  $z_3$ , we obtain for a given value of  $\vec{Q}$  a discrete set of mode frequencies  $\omega_n$  and corresponding perpendicular components  $k_n$  of the wave-vector. Each of these modes contributes to the stress tensor a quantity similar to that in Eq. (8), so that

$$-T_{zz}(z) = \frac{\hbar c}{2A} \sum_n \frac{f_n}{q_n} \left[ k_n^2 (|\phi_n^s|^2 + |\phi_n^p|^2) + (|\partial_z \phi_n^s|^2 + |\partial_z \phi_n^p|^2) \right]_z, \quad (\text{fixed } \vec{Q}), \quad (9)$$

where we have substituted the energy  $\mathcal{U}_n$  in terms of the equilibrium *occupation number*  $f_n = f(\omega_n) = \coth(\beta\hbar\omega_n/2)/2$  of a photon state with quantized energy  $\hbar\omega_n$  at temperature  $k_B T = 1/\beta$ , with  $k_B$  the Boltzmann's constant. The sum over states may be rewritten in terms of the tensorial Green's function  $\mathbf{G}(z, z')$  with components

$$G_{\vec{k}^2}^{\mu\nu}(z, z') = \sum_n \frac{\phi_n^\mu(z) \phi_n^{\nu*}(z')}{\vec{k}^2 - k_n^2}, \quad \mu, \nu = s, p, \quad (10)$$

for the 1D Helmholtz equation

$$\left(\partial_z^2 + \tilde{k}^2\right) G_{\tilde{k}^2}^{\mu\nu}(z, z') = \delta(z - z')\delta_{\mu\nu}. \quad (11)$$

Here,  $\tilde{k} = k + i\eta$ , ( $\eta > 0$ ), with the understanding that the limit  $\eta \rightarrow 0^+$  is to be taken at the end of the calculation. Using the identity  $\text{Im}(\tilde{k}^2 - k_n^2)^{-1} = -\pi\delta(k^2 - k_n^2)$ , we can replace the sum (9) by the integral

$$-T_{zz}(z) = \frac{\hbar c}{A} \int dk^2 \frac{f}{q} \rho_{\tilde{k}^2}, \quad (\text{fixed } \vec{Q}), \quad (12)$$

where  $f = f(\omega)$  and

$$\rho_{\tilde{k}^2}(z) = -\frac{1}{2\pi} \text{Im} \left( \tilde{k}^2 + \partial_z \partial_{z'} \right) \text{Tr} \mathbf{G}(z, z')|_{z=z'} \quad (13)$$

plays the role of a local density of states at  $z$  (number of states per unit length and per unit  $k^2$ ).

The solution of (11), subject to the appropriate boundary conditions, may be written in terms of the solutions  $\mathbf{u}(z)$  and  $\mathbf{v}(z)$  of the 1D Helmholtz equation that satisfy the boundary conditions on the right and left side of the system, respectively,

$$\begin{aligned} \mathbf{G}(z, z') &= \mathbf{u}(z) [\mathbf{u}'(z') - \mathbf{v}'(z') \mathbf{v}^{-1}(z') \mathbf{u}(z')]^{-1} \theta(z - z') \\ &\quad - \mathbf{v}(z) [\mathbf{v}'(z') - \mathbf{u}'(z') \mathbf{u}^{-1}(z') \mathbf{v}(z')]^{-1} \theta(z' - z), \end{aligned} \quad (14)$$

where  $\theta$  denotes the Heaviside unit step function. Here,  $\mathbf{u}(z)$  and  $\mathbf{v}(z)$  are  $2 \times 2$  matrices with matrix elements  $u_\lambda^\mu(z)$  and  $v_\lambda^\mu(z)$ ,  $\lambda = 1, 2$  denotes the two independent spinorial solutions of Helmholtz equation,  $\mu = s, p$  denotes their correspondent  $s$  and  $p$  components and  $\mathbf{u}'(z)$  and  $\mathbf{v}'(z)$  denote the derivatives of  $\mathbf{u}(z)$  and  $\mathbf{v}(z)$  with respect to their argument. We remark that we first introduced a similar expression for the spinorial Green's function in Ref. [48], where it was used to obtain the angular momentum flux within a 1D cavity.

The solutions  $\mathbf{u}(z)$  and  $\mathbf{v}(z)$  may be written within the cavity in terms of the reflection coefficients of the plates

$$\mathbf{r}_a = \begin{pmatrix} r_a^{pp} & r_a^{ps} \\ r_a^{sp} & r_a^{ss} \end{pmatrix}, \quad (a = 1, 2). \quad (15)$$

These are defined through

$$\xi_{r2}^\mu = \sum_\nu r_2^{\mu\nu} \xi_{i2}^\nu, \quad (16)$$

where we define the unnormalized spinors  $\xi_{i2}^\mu$  and  $\xi_{r2}^\mu$  ( $\mu = s, p$ ) as the amplitudes of the incident and reflected fields at the surface of plate 2 through

$$E_y(z) = \xi_{i2}^s e^{i\tilde{k}(z-L)} + \xi_{r2}^s e^{-i\tilde{k}(z-L)} \quad (17)$$

and

$$B_y(z) = \xi_{i2}^p e^{i\tilde{k}(z-L)} + \xi_{r2}^p e^{-i\tilde{k}(z-L)}. \quad (18)$$

The other components of the electromagnetic field may be obtained from Eqs. (17), (18) through Maxwell's curl equations. The matrix elements  $r_1^{\mu\nu}$  of plate 1 are similarly defined. Thus, we may write,

$$\mathbf{u}(z) = \mathbf{I} e^{i\tilde{k}(z-L)} + \mathbf{r}_2 e^{-i\tilde{k}(z-L)} \quad (19)$$

and

$$\mathbf{v}(z) = \mathbf{I} e^{-i\tilde{k}z} + \mathbf{r}_1 e^{i\tilde{k}z}, \quad (20)$$

where  $\mathbf{I}$  is the  $2 \times 2$  unit matrix.

Substitution of (19) and (20) in (14), (13) and (12) yields

$$-T_{zz} = \frac{\hbar c}{\pi A} \text{Re} \int dk^2 \frac{f \tilde{k}}{q \Delta} (1 - e^{4i\tilde{k}L} r_1 r_2), \quad (\text{fixed } \vec{Q}) \quad (21)$$

where  $r_a \equiv \det \mathbf{r}_a$  and

$$\Delta = \det (\mathbf{I} - e^{2i\bar{k}L} \mathbf{r}_1 \mathbf{r}_2). \quad (22)$$

Note that  $\Delta = 0$  yields the dispersion relation of the lossy modes of the real cavity.

Summing equation (21) over  $\vec{Q}$  we finally obtain

$$-T_{zz} = \frac{\hbar c}{2\pi^3} \int d^2Q \operatorname{Re} \int dk \frac{fk^2}{q\Delta} (1 - e^{4i\bar{k}L} r_1 r_2), \quad (23)$$

where we assumed Born-von Karman periodic boundary conditions along the surface of area  $A \rightarrow \infty$  to replace  $\sum_Q \dots \rightarrow A/(2\pi)^2 \int d^2Q \dots$ .

The flux of linear momentum  $-T_{zz}$  in the fictitious cavity is the same as in the real cavity between slabs 1 and 2. To obtain the force on slab 2, we have to subtract the flux in the real system between the slab and infinity. This can be obtained following the same derivation given above, but replacing the slab 1 by the complete system made up of slabs 1, the cavity  $\mathcal{V}$  and slab 2, and replacing slab 2 by empty space. The result is identical to equation (23), but substituting  $r_2 \rightarrow 0$ . Thus, the total force per unit area of slab 2 is

$$\begin{aligned} \frac{F_z}{A} &= \frac{\hbar c}{2\pi^3} \operatorname{Re} \int d^2Q \int dk f k^2 \frac{e^{2i\bar{k}L}}{q\Delta} \\ &\quad \times \left( \operatorname{Tr}(\mathbf{r}_1 \mathbf{r}_2) - 2e^{2i\bar{k}L} r_1 r_2 \right) \\ &= -\frac{\hbar c}{4\pi^3} \operatorname{Im} \int d^2Q \int dk f \frac{k}{q} \frac{d}{dL} \log \Delta \end{aligned} \quad (24)$$

The derivation above was performed for waves that propagate in vacuum, that is, within the light cone  $Q \leq \omega/c$  and for real  $k$ . For evanescent waves with  $Q > \omega/c$  and imaginary  $k$  the approach above has to be slightly modified, as it turns to be impossible to choose fictitious transmission amplitudes  $t_a^{\mu\nu}$  that guarantee energy conservation at the boundaries  $z_1$  and  $z_2$  of the fictitious cavity of Fig. 1. Nevertheless, the fictitious system may be easily altered to accommodate for evanescent waves [49], and it turns out that the expression (24) and (25) remain valid even outside of the light cone [49]. Thus, the integration region of Eq. (24) may include real and imaginary values of  $k$ , as long as the wavenumber  $q \equiv \omega/c = \sqrt{Q^2 + k^2}$  is real, i.e.,  $k$  should go along the imaginary axis from  $iQ$  to 0 and then along the real axis towards infinity.

The formalism developed above is a generalization to anisotropic systems of the formalism developed in Refs. [32–36] for the isotropic case. The resulting force (Eq. (24)) agrees with the usual Lifshitz's result expressed in terms of the reflection amplitudes in the isotropic case ( $r_a^{sp} = r_a^{ps} = 0$ ).

The potential energy  $U$  of the system may be now obtained by integrating the force (24) with respect to the plate separation from  $\infty$  towards the actual separation  $L$ , yielding

$$\frac{U}{A} = \frac{\hbar c}{4\pi^3} \operatorname{Im} \int d^2Q \int dk f \frac{k}{q} \log \Delta. \quad (25)$$

Notice that when  $L \rightarrow \infty$ ,  $\Delta \rightarrow 1$  as  $e^{2i\bar{k}L} \rightarrow 0$  for any positive of  $\eta$ . We make a change of variable from  $k$  to  $q$  and perform the usual rotation in the complex plane from the positive real axis towards the imaginary axis to rewrite Eq. (25) as

$$\frac{U}{A} = \frac{\hbar}{8\pi^3} \int_0^\infty du \int d^2Q \log \Delta \quad (26)$$

at  $T = 0$ , where we introduce an imaginary frequency  $\omega = iu$ , and as

$$\frac{U}{A} = \frac{k_B T}{4\pi^2} \operatorname{Re} \sum'_{\ell \geq 0} \int d^2Q \log \Delta_\ell \quad (27)$$

for  $T \neq 0$ , where we have accounted for the poles of  $f(iu)$  by performing residue-like integrations at the Matsubara frequencies  $u_\ell = 2\pi\ell k_B T/\hbar$  and we define  $\Delta_\ell = \Delta(\omega = iu_\ell)$ . The prime in the summation means that the  $\ell = 0$  term should be divided by 2. Eq. (26) coincides with that derived in Refs. [30, 31, 42] for  $T = 0$ .

Notice that for anisotropic plates, the matrices  $\mathbf{r}_a$  depend on their in-plane orientation. Therefore, the energy  $U$  (Eq. (25)) depends implicitly on the relative orientation  $\gamma$  between the optical axes of the plates. Thus, we expect a

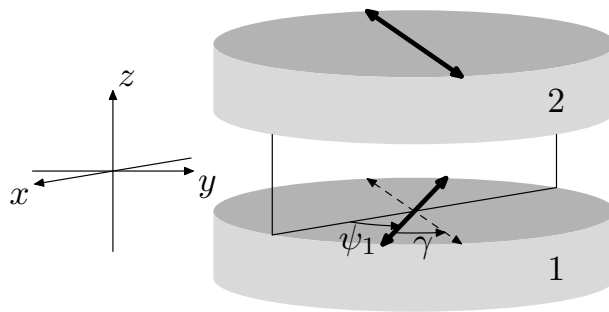


FIG. 2: Schematic diagram of the system, consisting of two parallel uniaxial non-magnetic plates whose optical axes lie on the surface. We indicate the optical axes of each plate with heavy double-headed arrows, and the projection of the axis of the second plate upon the first by a dashed double arrow. The  $z$ -axis is chosen to be orthogonal to the plates. We also indicate the plane of incidence. The angle  $\psi_1$  between the plane of incidence and the optical axis of plate 1 as well as the angle  $\gamma$  from the optical axis of plate 1 towards that of plate 2 are indicated. The angle  $\psi_2$  between the plane of incidence and the optical axis of plate 2 is  $\psi_2 = -\psi_1 - \gamma$ . The sign is due to the convention in Eq. (29).

torque  $M$  on the plates which we may calculate simply by taking the derivative  $M = -\partial U/\partial\gamma$ . It is easily verified that starting from Eq. (26) but setting  $\vec{Q} = 0$  instead of performing the integral  $(A/4\pi^2) \int d^2Q$  yields Eq. (13) of Ref. [48], i.e., the torque for a cavity in which the field is constrained to propagate along only one dimension, namely, along the normal to the surfaces. In ref. [48] the torque was obtained directly from the flux of angular momentum within the cavity. Here, we took a different approach, obtaining the torque from the angular dependence of the energy. The reason is that the angular momentum is well defined only for finite width beams and the overlap among the multiple reflections of a finite beam is incomplete for oblique incidence and ill defined for evanescent waves.

We remark that our results are written in terms of the optical coefficient matrices  $\mathbf{r}_a$  of the walls of the cavity, about which we have made no assumptions. Thus, our results may be applied to systems of arbitrary absorptance, conductivity and width, and they may be homogeneous or inhomogeneous. Up to this point the dependence of the energy, force and torque on the orientation of the plates has been implicit, through the unstated dependence of  $\mathbf{r}_a$ . In the next sections we will apply our result to specific cases where the dependence on  $\gamma$  can be exhibited explicitly.

### III. SEMI-INFINITE UNIAXIAL SLABS

We consider semi-infinite uniaxial non-magnetic crystals with their optical axes parallel to their surface. In this case, the reflection matrices  $\mathbf{r}_1$  and  $\mathbf{r}_2$  may be obtained as particular instances for surfaces 1 and 2 of the formula [50]

$$\mathbf{r} = (\mathbf{s}_2^{-1} + \mathbf{s}_1^{-1} \cos\theta)^{-1} (\mathbf{s}_1^{-1} \cos\theta - \mathbf{s}_2^{-1}), \quad (28)$$

which we derive in the appendix following the notation of Ref. [51]. Here,  $\mathbf{s}_1$  and  $\mathbf{s}_2$  are the  $2 \times 2$ -matrices

$$\mathbf{s}_1 = \begin{pmatrix} \frac{\tan\psi}{J} & -\frac{J^2 \cot\psi}{In_o} \\ 1 & 1 \end{pmatrix}, \quad \mathbf{s}_2 = \begin{pmatrix} \frac{n_o^2 \tan\psi}{J^2} & -\cot\psi \\ 1/J & n_o/I \end{pmatrix}, \quad (29)$$

and

$$\begin{aligned} I^2 &= n_o^2 n_e^2 - \sin^2\theta (n_o^2 \sin^2\psi + n_e^2 \cos^2\psi), \\ J^2 &= n_o^2 - \sin^2\theta, \end{aligned} \quad (30)$$

where  $n_o$  and  $n_e$  are the ordinary and extraordinary refractive indices of the uniaxial crystal,  $\theta$  is the angle of incidence and  $\psi$  is the angle from the plane of incidence to the optical axis of the crystal; its sign is chosen through the right hand rule around the normal of the surface that points outwards from the anisotropic medium. In Eqs. (29) we have assumed that the cavity is empty and thus we took its index of refraction of the cavity as 1.

Consider the sketch depicted in Fig. 2, which displays the angle  $\psi_1$  of the optical axis of plate 1 with respect to the plane of incidence and the angle  $\gamma$  between the optical axis of plate 2 and that of plate 1. According to our convention above, the angle  $\psi_2$  between the optical axis of plate 2 and the plane of incidence is  $\psi_2 = -\psi_1 - \gamma$ . We identify  $n_e = \sqrt{\epsilon_{\parallel}}$ ,  $n_o = \sqrt{\epsilon_{\perp}}$ , where  $\epsilon_{\parallel}$  and  $\epsilon_{\perp}$  are the dielectric response functions of the plates along and perpendicular to their optical axes, respectively. The substitution of equations (29), (30) in (28) and (27) yields after a tedious algebra

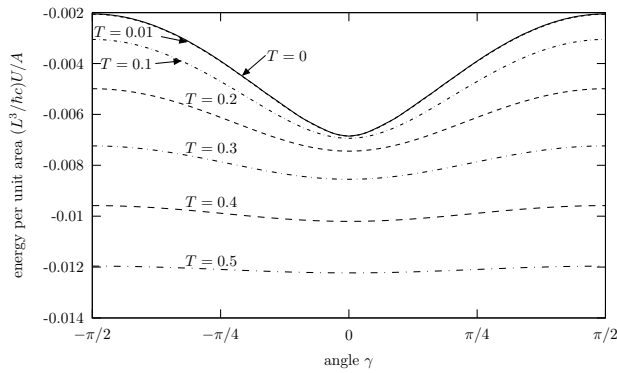


FIG. 3: Casimir energy per unit area  $U/A$  between two ideal uniaxial plates as a function of the angle  $\gamma$  between their optical axes for different temperatures  $T = 0, 0.01, 0.1, 0.2, 0.3, 0.4, 0.5$  in units of  $\hbar c/Lk_B$ .

an expression for the Casimir energy between anisotropic plates. We have checked that the resulting expression for  $\Delta$  coincide with that obtained in Ref. [25] for the same system. Nevertheless, the calculation of Ref. [25] is directly applicable only to local uniaxial semi-infinite homogeneous systems, as their calculation is setup in terms of the bulk dielectric function of the plates. On the other hand, our result is written in terms of the reflection amplitudes  $\mathbf{r}_a$  of the plates, and thus may be applied to any system for which we can calculate these optical coefficients, as shown explicitly in section IV.

Let us now consider an idealized case consisting of slabs which behave as perfect conductors along the optical axes but which are perfect insulators along the other principal directions. This could be realized through an array of perfectly conducting aligned wires insulated from each other. We further ignore the electric polarization across the wires, which would be appropriate, for example, if they were very thin. Then, each plate may be described by a dielectric response  $\epsilon_{\parallel} \rightarrow \infty$  and  $\epsilon_{\perp} \rightarrow 1$ . In this case the reflection matrix (28) becomes simply

$$\mathbf{r}(\theta, \psi) = \begin{bmatrix} \cos^2 \theta \cos^2 \psi & -\sin 2\psi \cos \theta/2 \\ \sin 2\psi \cos \theta/2 & -\sin^2 \psi \end{bmatrix} (1 - \sin^2 \theta \cos^2 \psi)^{-1}, \quad (31)$$

which yields

$$\Delta = 1 - \alpha^2 e^{2ikL} \quad (32)$$

when substituted into Eq. (22), where

$$\alpha^2 = \text{Tr}(\mathbf{r}_1 \mathbf{r}_2) = \frac{(\cos \gamma - \sin^2 \theta \cos \psi_1 \cos \psi_2)^2}{(1 - \sin^2 \theta \cos^2 \psi_1)(1 - \sin^2 \theta \cos^2 \psi_2)}. \quad (33)$$

Eqs. (32) and (33) were previously obtained for this system in Ref. [27], as becomes evident by writing the latter in terms of  $\varphi \equiv -\psi_2 = \psi_1 + \gamma$ .

Substitution of Eq. (32) into Eq. (26) yields the  $T = 0$  energy of the system. Fig. 3 shows our numerical results for the energy of the idealized system discussed above. We have verified that they agree with the results presented in Ref. [27] where a path integral approach [28, 29] was used. Nevertheless, a similar substitution into Eq. (27) permits us to calculate also the  $T \neq 0$  energy of the system, shown in the same figure. Notice that for this idealized case there is a natural temperature scale  $\hbar c/k_B L$  and a natural energy scale  $A\hbar c/L^3$ , as they are respectively intensive and extensive quantities with respect to the area  $A$  of the interfaces. We use these scales to normalize the units in the figure. As  $T$  increases, the Casimir energy becomes more negative, so that the plates are more strongly bound. However, the slope of the energy as a function of the angle, and thus, the torque, diminishes with increasing  $T$ . This result may appear somewhat surprising, as it is well known that increasing the temperature yields an increase of the magnitude of the Casimir force. For high enough temperatures the energy becomes independent of the angle and approaches its value at  $\gamma = 0$ , which is exactly half of the energy corresponding to two perfect isotropic mirrors. This can be easily verified by substituting  $\alpha^2 = 1$  into Eq. (32) and the resulting  $\Delta$  into (26) and (27).

The torque for the ideal case may now be simply calculated by analytically deriving under the integral sign the energy (26) or (27) with respect to the relative angle  $\gamma$  and performing the resulting integrals numerically. Fig. 4 shows that the torque  $M$  is a periodic function of  $\gamma$  with period  $\pi$ . It is null when the optical axes are aligned,  $\gamma = 0, \pi$ , corresponding to a stable equilibrium orientation. It is also null when they are orthogonal to each other,  $\gamma = \pm\pi/2$ ,



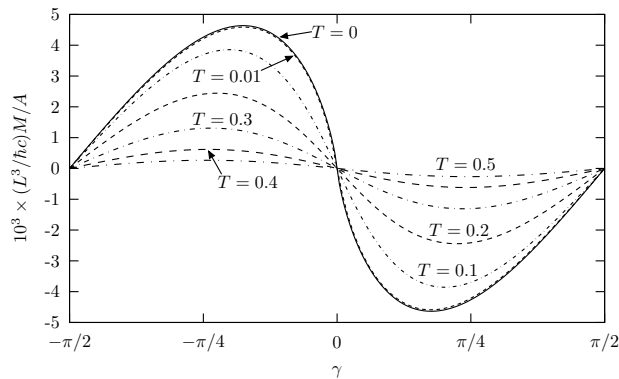


FIG. 4: Casimir torque per unit area  $M/A$  between two ideal uniaxial plates as a function of the angle  $\gamma$  between their optical axes. The torque is calculated for the same temperatures as in Fig. 3, expressed in units of  $\hbar c/Lk_B$ .

corresponding to an unstable equilibrium. For  $T = 0$  the slope of  $M(\gamma)$  seems singular at the stable equilibrium point. The existence of this singularity can actually be confirmed by deriving analytically the torque with respect to the angle  $\gamma$  under the integral sign and examining the integrand after having taken the corresponding limit  $\gamma \rightarrow 0$  and analytically performed the angular integral over  $\varphi$ . It turns out that the integrand has an infinite discontinuity at  $u = 0$ . This singularity had also been found previously in a 1D calculation [48], in which light is normally incident at the walls of the cavity. Furthermore, qualitatively the same behaviour of the torque as a function of the angle  $\gamma$  found in this 1D calculation, is obtained in the 3D calculation for  $T = 0$ . The torque is not simply proportional to  $\sin 2\gamma$ , so its extreme values are not at  $\gamma = \pm\pi/4$ . However, as the temperature increases the torque becomes more sinusoidal-like. Note that the maximum torque per unit area is of the order of  $M/A \sim 5 \times 10^{-3} \times \hbar c/L^3$ . Thus, for a separation  $L = 100$  nm, the maximum torque per area unit is about  $10^{-7}$  N/m. It is interesting to compare this result with that of Rodrigues et al. [41] for the case of two slightly misaligned corrugated metals. It has been argued [41] that that system would yield the largest torques. Nevertheless, we obtained a torque of the same order of magnitude as their's. Furthermore, in our case the torque remains large over a wide angular range, independently of the area of the system, while in their case the torque is significant only within a very small angular range which decreases with the size of the system.

Our theory may be applied to systems which are more realistic than the idealized case above. For example, in Fig. 5 we show the zero temperature torque between two uniaxial conductors whose response along the optical axis is characterized by the Drude dielectric function

$$\epsilon_{\parallel}(\omega) = 1 - \frac{\omega_p^2}{\omega^2 + i\omega/\tau}. \quad (34)$$

For simplicity, we assume they do not respond along the perpendicular direction,  $\epsilon_{\perp} = 1$ , as could correspond to parallel plates made up of an array of very thin aligned wires, each of which is a conductor with a finite Drude-like conductivity. We include results for different values of the electronic density and therefore of the plasma frequency  $\omega_p$ , as well as the ideal limit  $\omega_p \rightarrow \infty$ . In the figure we used  $\omega_0 = \pi c/L$  as a natural frequency scale and we chose the electronic lifetime  $\tau = 10^3/\omega_0$  which would correspond to a typical values within a metal for  $L \sim 10^2$  nm, although the results are very insensitive to  $\tau$ . In this case,  $\omega_0$  would be of the order of a typical metallic plasma frequency.

When  $\omega_p \gg \omega_0$  the plates behave as perfect mirrors and, as verified by Fig. 5, we recover the idealized case studied above, including the approach to the singularity in the slope at  $\gamma = 0$ . As expected, the torque increases with  $\omega_p$  and becomes null at  $\omega_p = 0$ .

#### IV. FILMS

Our formalism, summarized by Eqs. (26) and (27), is written entirely in terms of the reflection amplitudes  $\mathbf{r}_1$  and  $\mathbf{r}_2$  of the anisotropic plates through Eq. (22). This has the enormous advantage over previous formalisms [21, 25, 26] in that different systems may be explored simply by substituting their corresponding reflection amplitudes. For arbitrary uniaxial systems we could simply substitute the ordinary and extraordinary indices of refraction in the formulae derived in the previous section. In this section we further illustrate the versatility of our theory by calculating the torque between two anisotropic dielectric plates one of which is a film with finite thickness  $d$ . For the reflection amplitudes

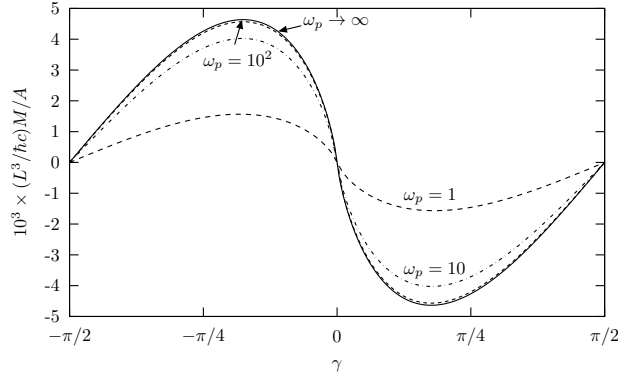


FIG. 5: Casimir torque at  $T = 0$  between two uniaxial plates as a function of the angle  $\gamma$  between their optical axes. The plates are conducting along their optical axis with a response  $\epsilon_{\parallel}$  described by a Drude dielectric function with a relaxation time  $\tau$ , and a plasma frequency  $\omega_p$ , and we assume the response perpendicular to the optical axis is  $\epsilon_{\perp} = 1$ . We chose a fixed value  $\tau = 1000/\omega_0$ , and we show results for various values of  $\omega_p = 1, 10$  and  $10^2 \times \omega_0$  where  $\omega_0 = \pi c/L$ . We also include the case  $\omega_p = \infty$  corresponding to the ideal case studied above.

$\mathbf{r}_1$  of the semi-infinite plate, which we take to be plate 1, we can simply use Eq. (28), but we have to calculate the reflection coefficients  $\mathbf{r}_2$  of the film.

Consider the reflection of an arbitrary polarized plane-wave with frequency  $\omega$  from an uniaxial anisotropic free-standing homogeneous dielectric film of finite thickness  $d$ , with its optical axis parallel to its surface. We assume that the system is described by the same geometry as in the previous section, illustrated by Fig. 2, and that the film is non-magnetic.

For each frequency  $\omega$  and parallel projection  $\vec{Q}$  of the wave-vector, two types of waves coexist inside the film, the *ordinary* and *extraordinary* waves, each of which has a wave vector component  $\pm k_{\mu}$  normal to the surface, where  $\mu = o$  for ordinary waves,  $\mu = e$  for extraordinary waves and we choose the upper sign for waves travelling or decaying towards  $z$ , i.e., we choose  $k_{\mu}$  as the solution of the dispersion relation that is consistent with  $\text{Im}(k_{\mu}) > 0$  for evanescent waves and for propagating waves in the presence of finite or infinitesimal absorption. This gives a total of four waves in the film. Thus, we describe the electromagnetic field within the film as [51]

$$\mathbf{F}(z) = \sum_{\sigma, \mu} \psi_{\sigma}^{\mu} \mathbf{V}_{\sigma}^{\mu} e^{i\sigma k_{\mu} z}, \quad (35)$$

where  $\mathbf{F}$  is a 4-component column vector which contains the electric and magnetic field projections parallel to the surface,  $\mathbf{F} = (E_x, B_y, E_y, -B_x)^T$ ,  $\psi_{\sigma}^{\mu}$  is the amplitude of the normal mode propagating in the  $\sigma z$  direction ( $\sigma = +, -$ ) with polarization  $\mu = o, e$ , while  $\mathbf{V}_{\sigma}^{\mu}$  is the eigenvector describing the electromagnetic field  $\mathbf{F}$  of a single mode with propagation direction  $\sigma$  and polarization  $\mu$ , and  $\sigma k_{\mu} = \pm k_{\mu}$  is the component of the corresponding wave-vector along  $z$  (see the appendix for details).

The field reflected by the film has two contributions. One of them is the field reflected by its front surface. The other is the field transmitted back into the cavity from the film, after having entered the film from the cavity and being multiply reflected. Thus, we may write

$$\mathbf{r}_2 \boldsymbol{\xi}_{i2} = \mathbf{r}_{02} \boldsymbol{\xi}_{i2} + \mathbf{t}_{20} \boldsymbol{\psi}_{-} \quad (36)$$

where  $\boldsymbol{\psi}_{\sigma} = (\psi_{\sigma}^o, \psi_{\sigma}^e)^T$  is a 2-component column vector containing the total  $o$  and  $e$  amplitudes of the waves travelling in the  $\sigma z$ -direction within the film,  $\boldsymbol{\xi}_{i2} = (\xi_{i2}^p, \xi_{i2}^s)^T$  is the vector containing the  $p$  and  $s$  contributions of the incident field and is defined through Eqs. (17)-(18), the matrix  $\mathbf{r}_2$  is the sought reflection amplitude of the film,  $\mathbf{r}_{02}$  is the reflection amplitude of the front surface when light impinges from the cavity and therefore it is given by Eq. (28), and  $\mathbf{t}_{20}$  is the transmission amplitude from the film into the cavity across the front surface. Similarly, the field that travels towards  $z$  within the film is the sum of the field transmitted from the cavity into the film plus the field travelling towards  $-z$  and internally reflected back at the front surface, so we may write

$$\boldsymbol{\psi}_{+} = \mathbf{t}_{02} \boldsymbol{\xi}_{i2} + \mathbf{r}_{20} \boldsymbol{\psi}_{-}, \quad (37)$$

where  $\mathbf{t}_{02}$  is the transmission amplitude from the cavity into the film through the front surface, and  $\mathbf{r}_{20}$  is the internal reflection amplitude of the front surface when light impinges from within the film. Similarly, at the rear surface, we

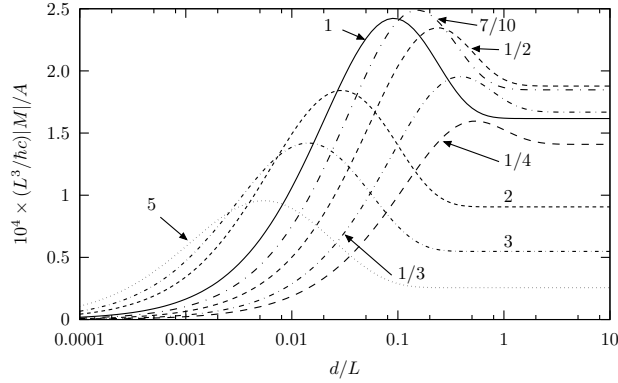


FIG. 6: Casimir torque at  $T = 0$  between a semi-infinite uniaxial, dissipation-less conducting slab and a film made up of the same material as a function of thickness  $d$  of the film. The slabs are modelled as Drude metals with a plasma frequency  $\omega_{p\parallel}$  along the optical axis twice as large than its value  $\omega_{p\perp}$  along the perpendicular direction. The curves are labelled by the value of  $\omega_{p\perp}/\omega_0 = 1/4, 1/3, 1/2, 7/10, 1, 2, 3, 5$ , where  $\omega_0 = \pi c/L$ . We fixed the relative angle between the optical axes at  $\gamma = \pi/4$ .

may write

$$\boldsymbol{\kappa}^{-1}\boldsymbol{\psi}_- = \mathbf{r}_{20}\boldsymbol{\kappa}\boldsymbol{\psi}_+ \quad (38)$$

where  $\boldsymbol{\kappa} = \text{diag}(e^{ik_o d}, e^{ik_e d})$  is a  $2 \times 2$  diagonal matrix that accounts for the phase acquired by the ordinary and extraordinary waves as they travel from the front surface towards the rear surface of the film. Notice that the internal reflection matrix of the rear interface coincides with the internal reflection matrix at the front interface as we consider a free standing film, and hence we denote both matrices by  $\mathbf{r}_{20}$ . Elimination of  $\boldsymbol{\psi}_+$  and  $\boldsymbol{\psi}_-$  from Eqs. (36)-(38) yields

$$\mathbf{r}_2 = \mathbf{r}_{02} + \mathbf{t}_{20}\boldsymbol{\kappa}\mathbf{r}_{20}\boldsymbol{\kappa}(\mathbf{I} - (\mathbf{r}_{20}\boldsymbol{\kappa})^2)^{-1}\mathbf{t}_{02}. \quad (39)$$

We remark that the same result would be obtained by generalizing Airy's method [52], summing the amplitudes of successive multiple reflections and refractions, but taking account of their  $2 \times 2$ -tensorial character due to the mixing of polarizations at the interfaces. Equivalent results may also be obtained through a  $4 \times 4$  transfer matrix formalism [51, 53], though care must be taken to avoid numerical instabilities. The calculation of the required matrices  $\mathbf{t}_{02}$ ,  $\mathbf{t}_{20}$ , and  $\mathbf{r}_{20}$ , as well as the calculation of the wave vector components  $k_\mu$  is shown in the Appendix.

By substituting Eq. (39) into Eqs. (26) or (27) we finally obtain the Casimir energy corresponding to an anisotropic film in front of a semi-infinite, anisotropic substrate. Then, the torque is obtained as before, simply by deriving analytically the energy under the integral sign with respect to the angle  $\gamma$  between the optical axes.

In Fig. 6 we show the torque between a semi-infinite anisotropic substrate and an anisotropic film as a function of the thickness  $d$  of the film. The substrate and the film are made of the same material which we assume is an uniaxial conductor with different plasma frequencies along its principal directions, i.e., with a tensorial anisotropic effective mass, and which we model by a Drude-like response along and perpendicular to the optical axis

$$\epsilon_\mu(\omega) = 1 - \frac{\omega_{p\mu}^2}{\omega^2 + i\omega/\tau}, \quad \mu = \perp, \parallel. \quad (40)$$

We include results for different values of  $\omega_{p\perp}$  for a fixed quotient  $\omega_{p\parallel}/\omega_{p\perp} = 2$  and for simplicity, we disregarded the dissipation, assuming  $\tau = \infty$ .

From Fig. 6 we see that for very thin films the torque becomes smaller as the normalized film thickness  $d$  becomes smaller and eventually the torque becomes null for a zero film thickness  $d \rightarrow 0$ , as  $\mathbf{r}_2 \rightarrow 0$  vanishes in that limit, as can be verified from Eq. (39). For large enough values of  $d$  the torque tends to its asymptotic value corresponding to semi-infinite plates. Curiously, the figure shows optimal values of the film thickness for which the torque is maximized. For the chosen parameters, the maximum torque may be as large as twice its asymptotic value. The optimal thickness shifts towards smaller values as the plasma frequency  $\omega_{p\perp}$  is increased. Furthermore, the magnitude of the torque at the optimal thickness is maximum for values of  $\omega_{p\perp}$  around  $\omega_0$ .

In order to explain qualitatively the results shown in Fig. 6, we consider a 1D model in which light is normally incident at the walls of the cavity. In this case, it is possible to decouple the ordinary and extraordinary rays inside the media by choosing the polarization of the incident electrical field. Light polarized in the directions normal or

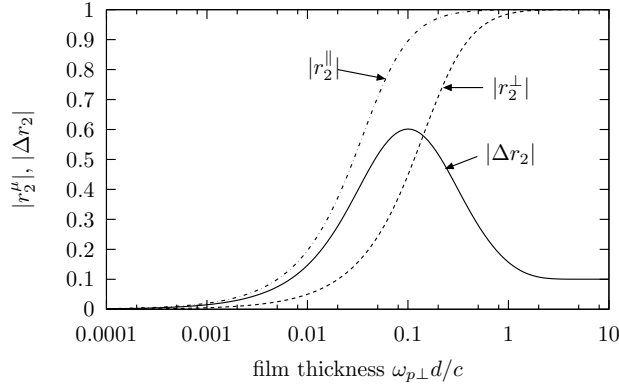


FIG. 7: Magnitude of the normal-incidence reflection coefficients  $|r_2^\mu|$  of an anisotropic, thin, dissipation-less Drude conducting film with plasma frequencies  $\omega_{p\parallel} = 2\omega_{p\perp}$ , and magnitude of the reflection anisotropy  $|\Delta r_2|$  as a function of the film thickness  $d$ . The frequency is  $\omega = 0.1\omega_{p\perp}$ .

parallel to the optical axis will only excite the ordinary or extraordinary wave inside the media and will be reflected without changing its polarization with reflection amplitudes  $r^\perp$  or  $r^\parallel$  respectively. The torque at  $T = 0$  for this one dimensional system can be calculated using the results of Ref. [48],

$$M = -\frac{\hbar \sin 2\gamma}{2\pi} \int_0^\infty du \frac{\Delta r_1 \Delta r_2 e^{-2uL/c}}{\Delta r_1 \Delta r_2 \sin^2 \gamma e^{-2uL/c} + (1 - r_1^\parallel r_2^\parallel e^{-2uL/c})(1 - r_1^\perp r_2^\perp e^{-2uL/c})}, \quad (41)$$

where  $\Delta r_a = r_a^\parallel - r_a^\perp$ . The reflection coefficients are [54]

$$r_1^\mu = \frac{1 - \sqrt{\epsilon_\mu}}{1 + \sqrt{\epsilon_\mu}} \quad (42)$$

for plate 1, and [54]

$$r_2^\mu = r_1^\mu \frac{1 - e^{2ik_\mu d}}{1 - (r_1^\mu)^2 e^{2ik_\mu d}} \quad (43)$$

for the film, where  $\mu = \parallel, \perp$  and  $k_\mu = \sqrt{\epsilon_\mu} \omega/c$  is the wave number inside the film corresponding to  $\mu$ -polarization.

According to Eq. (41), we might understand the dependence of the torque  $M$  on the thickness  $d$  of the film if we first understand the dependence of the anisotropy  $\Delta r_2$  on  $d$ . Consider first a wave of frequency  $\omega > \omega_{p\perp}, \omega_{p\parallel}$ , normally incident on the film 2. In this case, the film would be transparent for both polarizations and the anisotropy would be small. For intermediate frequencies,  $\omega_{p\perp} < \omega < \omega_{p\parallel}$ , the film would be a good reflector for one polarization and transparent for the perpendicular polarization, yielding a large anisotropy which nevertheless would be quite insensitive to the thickness of the film. However, for  $\omega < \omega_{p\perp} < \omega_{p\parallel}$  the penetration depth  $\ell_\perp$  for polarization perpendicular to the optical axis would be larger than the penetration depth  $\ell_\parallel$  for polarization along the optical axis. For a sufficiently thick film,  $d > \ell_\perp > \ell_\parallel$  and the film would be a good reflector for both polarizations as no radiation would get across it, so the anisotropy would be small. For a sufficiently thin film  $\ell_\perp > \ell_\parallel > d$ , the radiation would reach the back surface and leave the film, which would be a poor reflector for both polarizations and thus the anisotropy would again be small. In the limit of vanishing thickness  $d \rightarrow 0$  all the incident radiation would be transmitted through the film and none reflected. Nevertheless, for an intermediate thickness such that  $\ell_\perp > d > \ell_\parallel$  the film would be a good reflector for polarization along the optical axis but a poor reflector along the perpendicular direction, yielding a large anisotropy.

These qualitative features are displayed in Fig. 7, where we show the magnitude of the reflection coefficients  $|r_2^\mu|$  as well as the magnitude of the anisotropy  $|\Delta r_2|$  as a function of  $d$  for the case  $\omega = 0.1\omega_{p\perp}$ . In the limit of large thickness  $d \gg c/\omega_{p\perp}$ , the anisotropy of the film  $\Delta r_2$  tends to its asymptotic value, which is non zero due to the relative phase between the complex optical coefficients corresponding to both polarizations. The film thickness  $d^m$  which maximizes the anisotropy can be calculated from Eq. (43) in a straightforward way, yielding

$$d^m \approx \frac{2|\omega|c}{\omega_{p\perp}\omega_{p\parallel}}, \quad |\omega| < \omega_{p\perp}, \omega_{p\parallel} \quad (44)$$

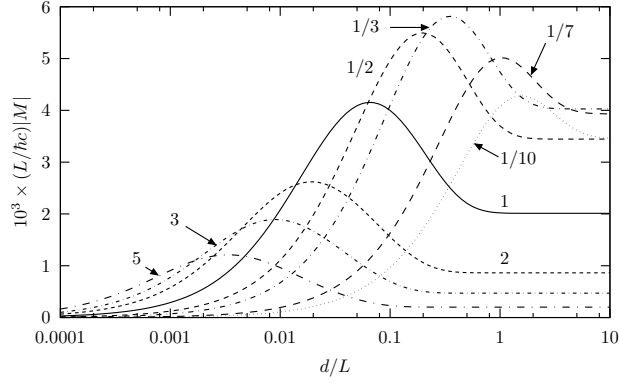


FIG. 8: Casimir torque 1D (only light normally incident is accounted for) at  $T = 0$  of the same system considered in Fig. 6, as a function of the thickness of the film  $d/L$ . The torque is calculated for  $\omega_{p\perp} = \omega_p = 1/10, 1/7, 1/3, 1/2, 1, 2, 3, 5$  (in units of  $\omega_0 = \pi c/L$ ). The rest of the parameters are the same as in Fig. 6.

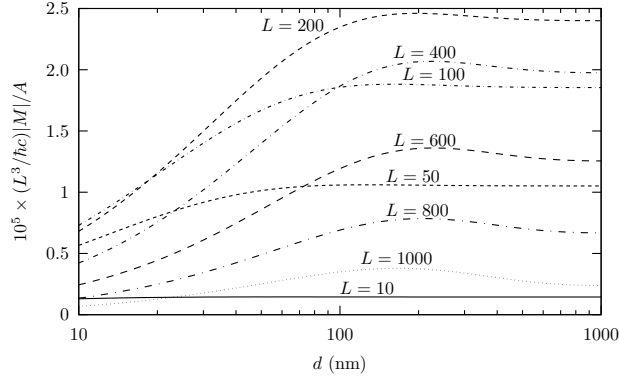


FIG. 9: Casimir torque at  $T = 0$  between a semi-infinite substrate of  $\text{TiO}_3$  and a film of calcite, as a function of the thickness of the film  $d$ . The torque is calculated for several separations  $L = 10, 50, 100, 200, 400, 600, 800, 1000$  nm. The angle between the optical axes is  $\gamma = \pi/4$ .

for small real or imaginary frequency.

In Fig. 8 we show the torque as a function of the width  $d$  for the same system as in Fig. 6 but assuming that the field propagates only in 1D [48]. The results display the same qualitative behavior as in the 3D case, although the plasma frequency  $\omega_{p\perp}$  for which the magnitude of the torque attains its maximum is shifted to a smaller value  $\omega_{p\perp}/\omega_0 \approx 1/3$  compared to  $7/10$  in Fig. 6. We may estimate the optimal width for each value of  $\omega_{p\perp}$  through the following considerations: The exponential in Eq. (41) suppresses the contribution of large imaginary frequencies  $u > c/2L$  to the Casimir effect. Thus, in the retarded regime  $\omega_{p\perp} > \omega_0$  we may consider mostly low imaginary frequencies  $u/\omega_{p\mu} < 1$  to understand the effect. Furthermore, as the relevant frequency scale is  $c/L \sim \omega_0/\pi$ , then the localization of the optimal film thickness in the retarded regime could be estimated by substituting  $|\omega| = u = \omega_0/\pi$  within Eq. (44). Thus, we obtain  $d^m/L \approx 0.025, 0.01$  and  $0.004$  for the choices  $\omega_{p\perp}/\omega_0 = 2, 3$  and  $5$  respectively. These estimates are in good agreement with the 1D calculation, Fig. 8. In the 3D case one would have to take into account modes that propagate along non-normal directions. However, as the reflection amplitude increases towards unity for any polarization as the angle of incidence moves away from the normal direction, the anisotropy in the reflectance and the corresponding contribution to the torque also diminish. Thus, the most important contributions to the torque come from modes that propagate close to the normal and our estimates for  $d^m$  are also in good qualitative agreement with our full 3D calculation, Fig. 6.

The simple estimates above fail in the non-retarded regime  $\omega_{p\perp} < \omega_0$  for both the 1D and 3D calculation, as in this case a wider range of frequencies, going beyond  $\omega_{p\perp}, \omega_{p\parallel}$ , contributes to the torque. Furthermore, for small separations  $L$  the Casimir effect in the 3D case is dominated by surface plasmons [55] which are completely left out of the 1D calculation and of our estimates above.

To conclude this section, in Fig. 9 we show the Casimir torque between a crystal of  $\text{BaTiO}_3$  and a crystal of calcite,

as in Ref. [24]. However, instead of two semi-infinite crystals, we consider a thin calcite film over a semi-infinite BaTiO<sub>3</sub> substrate with vacuum in between and we vary the thickness  $d$  of the film. We use the same model as in Ref. [24] to describe the dielectric response of the plates along each of their principal directions, namely, two undamped oscillators [56] to account for both the IR and UV resonances. We show results for  $T = 0$  which we expect to hold even at room temperature for separations in the range  $L < 1\mu\text{m}$ . We have confirmed that our numerical results, performed at  $T = 0$ , are in agreement with those of Ref. [24] in the limit of very thick plates.

As expected, Fig. 9 shows that for very thin films the torque becomes null, while for thick enough films it attains its asymptotic value corresponding to semi-infinite plates. Fig. 9 displays small maxima corresponding to an optimal thickness for which the torque is maximized for each value of the separation, analogous to those found above for anisotropic conducting films, although these maxima are very broad. In this case, the maximum torque is about one order of magnitude smaller than for the case of anisotropic conductors shown in Fig. 6 when typical metallic plasma frequencies are chosen, and about two orders of magnitude smaller than for the case of the ideal uniaxial plates shown in Fig. 4.

In order to observe the Casimir torque, several experimental setups have been suggested [24, 57]. If the vacuum Casimir cavity is replaced by a cavity filled with a dielectric liquid, and if the dielectric function of the fluid is intermediate between that of the cavity walls, then the sign of the Casimir force may be reversed, becoming repulsive instead of attractive. Munday et al. [24] took advantage of this sign reversal and estimated that a quartz or calcite anisotropic disk with a diameter and a width of some tens of  $\mu\text{m}$  would float at a height of about one hundred  $\text{nm}$  over the surface of a barium titanate anisotropic crystal if immersed in ethanol. At this height, the repulsive Casimir force would balance the weight of the disk, which would then be able to rotate freely around its axis. Then it would be possible to first align the disk with the polarization of a laser beam and optically monitor the rotation towards the equilibrium orientation after the laser beam is turned off. The characteristic time would depend of the viscosity of the fluid and on the magnitude of the driving Casimir torque which would thus be obtained.

In a second proposal by the same group [57] a large set of much smaller disks of  $\mu\text{m}$  scale width and diameter are kept separated a few nanometers from the substrate not by a repulsive Casimir force but by surfactant molecules that attach to the surfaces of both the substrate and the disks which in this case would be immersed in an electrolyte. The orientation of such small disks would be disrupted by their rotational Brownian motion, but the distribution of their orientations would yield \*\*\*\* Sepasuchi.

According to our calculations above, structured materials made up of aligned nanowires embedded in dielectric matrices are subject to much larger torques than the birefringent crystals considered by Munday et al. [24, 57]. Thus, the Casimir torque could be measured using a torsion balance. To avoid alignment problems, a spherical anisotropic particle could be used instead of a flat disk. Hanging a 50  $\mu\text{m}$  sphere from a 10  $\mu\text{m}$  long aluminum wire of 50  $\text{nm}$  radius

frecuencia =100Hz vacío placa giratoria. 50HZ.

## V. CONCLUSIONS

We have extended a fictitious-cavity approach to calculate the Casimir force, energy and torque between anisotropic media with a planar geometry in terms only of their optical coefficients. Our results are applicable to arbitrary anisotropic materials which may be conducting or insulating, opaque or transparent, semi-infinite or with a finite thickness, with a non-dispersive or a frequency dependent response, homogeneous or structured, as long as we can calculate their corresponding reflection coefficients. Our expressions for the torque were simply obtained by analytically deriving the energy with respect to the relative orientation of the plates. The formalism has allowed us to perform calculations at zero and at finite temperature.

We have reproduced some known results and we have calculated the torque for ideal uniaxial systems which are the anisotropic counterparts to the ideal Casimir mirrors, namely, systems which are perfect conductors along some directions and perfect insulators along others. We also calculated the torque for systems with a Drude conductivity. As a non trivial application of our formalism, we have calculated the torque for a system consisting of two anisotropic slabs, one of which is a semi-infinite substrate and the other a thin film of thickness  $d$ . The slabs were modelled as Drude metals and made up of the same material in order to study the effect of the film thickness in the torque. Our numerical results show that exists an optimal value of the film thickness where the torque is maximized. We have estimated the optimal thickness in the retarded regime by studying the anisotropy of the skin depth evaluated at the characteristic frequency of the cavity; the maximum torque is achieved for films whose thickness is intermediate between the largest and the smallest of the two principal skin depths. Finally, we calculated the Casimir torque for a thin film of calcite above a barium titanate substrate. The results seem qualitatively similar although the torque is smaller than that for uniaxial conductors and for the ideal system.

In conclusion, we developed a very general formalism to calculate the Casimir torque and illustrated its use by

studying the torque at zero and finite temperatures for ideal and realistic, conducting and insulating systems of semi-infinite and finite widths. We expect that the simplicity and generality of our formalism motivates further studies of these relatively unexplored aspects of the Casimir effect between anisotropic media.

### Acknowledgments

This work was partially supported by DGAPA-UNAM under grant IN120909.

### Appendix

In this appendix we derive the expressions for the matrices  $\mathbf{t}_{20}$ ,  $\mathbf{r}_{20}$ ,  $\mathbf{t}_{02}$  and the  $z$ -component of the wave-vectors of the ordinary and extraordinary waves. We derive these expressions by following the method developed in Refs. [51, 53]. We assume that the system is described by the geometry shown in Fig. 2. Thus, the dielectric tensor is given by

$$\epsilon = \begin{bmatrix} \epsilon_{\parallel} \cos^2 \psi + \epsilon_{\perp} \sin^2 \psi & (\epsilon_{\perp} - \epsilon_{\parallel}) \sin \psi \cos \psi & 0 \\ (\epsilon_{\perp} - \epsilon_{\parallel}) \sin \psi \cos \psi & \epsilon_{\perp} \cos^2 \psi + \epsilon_{\parallel} \sin^2 \psi & 0 \\ 0 & 0 & \epsilon_{\perp} \end{bmatrix}. \quad (45)$$

All of the quantities above (the dielectric functions and the angles) refer to plate 2, but we omit the corresponding index (2) in order to simplify our notation. On the other hand, from Maxwell equations, the components of the electromagnetic field parallel to the  $x - y$  plane, can be cast in a set of four differential equations

$$\partial_z \mathbf{F} = iq\mathbf{\Gamma} \mathbf{F}, \quad (46)$$

where

$$\mathbf{F} = (E_x, B_y, E_y, -B_x)^T, \quad (47)$$

$E_x$ ,  $E_y$ ,  $B_x$  and  $B_y$  are the electric and magnetic field components parallel to the interfaces,  $q$  is the free-space wavenumber and  $\mathbf{\Gamma}$  is a  $4 \times 4$  matrix with elements

$$\begin{aligned} \Gamma_{11} &= -\sin \theta \epsilon_{zx} / \epsilon_{zz}, \\ \Gamma_{12} &= 1 - \sin^2 \theta / \epsilon_{zz}, \\ \Gamma_{13} &= -\sin \theta \epsilon_{zy} / \epsilon_{zz}, \\ \Gamma_{14} &= \Gamma_{24} = \Gamma_{31} = \Gamma_{32} = \Gamma_{33} = \Gamma_{44} = 0, \\ \Gamma_{21} &= \epsilon_{xx} - \epsilon_{xz} \epsilon_{zx} / \epsilon_{zz}, \\ \Gamma_{22} &= -\sin \theta \epsilon_{xz} / \epsilon_{zz}, \\ \Gamma_{23} &= \epsilon_{xy} - \epsilon_{xz} \epsilon_{zy} / \epsilon_{zz}, \\ \Gamma_{34} &= 1, \\ \Gamma_{41} &= \epsilon_{yx} - \epsilon_{yz} \epsilon_{zx} / \epsilon_{zz}, \\ \Gamma_{42} &= \sin \theta \epsilon_{yz} / \epsilon_{zz}, \\ \Gamma_{43} &= \epsilon_{yy} - \sin^2 \theta - \epsilon_{yz} \epsilon_{zy} / \epsilon_{zz}. \end{aligned} \quad (48)$$

where  $\theta$  is the angle of incidence. Within a homogeneous medium  $\mathbf{\Gamma}$  is independent of  $z$  and Eq. (46) has four particular solutions of the form

$$\mathbf{F} = \mathbf{F}_{\ell}(0) e^{ik_{\ell} z}, \quad \ell = 1, 2, 3, 4, \quad (49)$$

where  $k_{\ell}$  is the component of the propagation vector parallel to the  $z$ -axis. Substitution of Eq. (49) into the Eq. (46) yields the eigenvalue equation

$$(k_{\ell} \mathbf{I} - q\mathbf{\Gamma}) \mathbf{F}_{\ell}(0) = 0 \quad (50)$$

whose eigenvalues

$$k_{\ell} = \pm k_o, \pm k_e \quad (51)$$

are

$$k_o = Jq, \quad (52)$$

$$k_e = Iq/\sqrt{\epsilon_\perp}, \quad (53)$$

where the quantities  $I$  and  $J$  are defined by Eqs. (30). The corresponding four eigenvectors are

$$\mathbf{V}_\pm^o = \begin{pmatrix} \pm \tan \psi / J \\ \epsilon_\perp \tan \psi / J^2 \\ \pm 1 / J \\ 1 \end{pmatrix}, \quad \mathbf{V}_\pm^e = \begin{pmatrix} \mp \frac{J^2 \cot \psi}{I\sqrt{\epsilon_\perp}} \\ -\cot \psi \\ \pm \sqrt{\epsilon_\perp} / I \\ 1 \end{pmatrix}, \quad (54)$$

where the eigenvector  $\mathbf{V}_\sigma^\mu$  describes the  $\mu$ -polarized wave with a wave vector component  $\sigma k_\mu$  along the  $z$ -axis.

Consider the reflection of light impinging at the interface between vacuum and a semi-infinite anisotropic medium from within the medium. The electromagnetic field at the vacuum side is made up of only a transmitted wave. Inside the medium, the electromagnetic field is made up of four waves  $\mathbf{F} = \sum_{\sigma,\mu} \psi_\sigma^\mu \mathbf{V}_\sigma^\mu e^{i\sigma k_\mu z}$ . The field  $\mathbf{F}$  is continuous across the interface, thus

$$\mathbf{F}_t = \sum_{\sigma,\mu} \psi_\sigma^\mu \mathbf{V}_\sigma^\mu e^{i\sigma k_\mu z}. \quad (55)$$

Writing the generalized vector field  $\mathbf{F}_t$  in terms of the spinor  $\boldsymbol{\xi}_t = (\xi_t^p, \xi_t^s)^T$ , defined through Eqs. (17)-(18), when they are applied to the transmitted field, we get

$$\mathbf{F}_t = (-\xi_t^p \cos \theta, \xi_t^p, \xi_t^s, -\xi_t^s \cos \theta)^T. \quad (56)$$

Substitution of this equation into Eq. (55) yields four linear algebraic equations that can be recast as two matrix equations for the spinors  $\boldsymbol{\xi}_t$  and  $\boldsymbol{\psi}_\pm = (\psi_\pm^o, \psi_\pm^e)^T$ ,

$$-\cos \theta \boldsymbol{\xi}_t = \mathbf{s}_1 \boldsymbol{\psi}_+ + \mathbf{s}_3 \boldsymbol{\psi}_- \quad (57)$$

and

$$\boldsymbol{\xi}_t = \mathbf{s}_2 \boldsymbol{\psi}_+ + \mathbf{s}_4 \boldsymbol{\psi}_-, \quad (58)$$

where  $\mathbf{s}_1$  and  $\mathbf{s}_2$  are the  $2 \times 2$ -matrices

$$\mathbf{s}_1 = \begin{pmatrix} V_{1,+}^o & V_{1,+}^e \\ V_{4,+}^o & V_{4,+}^e \end{pmatrix}, \quad \mathbf{s}_2 = \begin{pmatrix} V_{2,+}^o & V_{2,+}^e \\ V_{3,+}^o & V_{3,+}^e \end{pmatrix}, \quad (59)$$

here,  $V_{i,\sigma}^\mu$  is the  $i$ -th component of the eigenvector  $V_\sigma^\mu$  given by Eqs. (54) and when these are substituted in Eqs. (59) yield the same expressions than those of Eqs. (29). Similarly,  $\mathbf{s}_3$  and  $\mathbf{s}_4$  are the matrices

$$\mathbf{s}_3 = \begin{pmatrix} V_{1,-}^o & V_{1,-}^e \\ V_{4,-}^o & V_{4,-}^e \end{pmatrix}, \quad \mathbf{s}_4 = \begin{pmatrix} V_{2,-}^o & V_{2,-}^e \\ V_{3,-}^o & V_{3,-}^e \end{pmatrix}. \quad (60)$$

Elimination of  $\boldsymbol{\xi}_t$  from Eqs. (57)-(58) yields

$$\boldsymbol{\psi}_+ = -(\mathbf{s}_1 + \mathbf{s}_2 \cos \theta)^{-1} (\mathbf{s}_3 + \mathbf{s}_4 \cos \theta) \boldsymbol{\psi}_-. \quad (61)$$

Thus, from  $\boldsymbol{\psi}_+ = \mathbf{r}_{20} \boldsymbol{\psi}_-$  we obtain

$$\mathbf{r}_{20} = -(\mathbf{s}_1 + \mathbf{s}_2 \cos \theta)^{-1} (\mathbf{s}_3 + \mathbf{s}_4 \cos \theta). \quad (62)$$

The matrix  $\mathbf{t}_{20}$  can be obtained by substituting Eq. (61) into Eq. (58) to get

$$\boldsymbol{\xi}_t = (\mathbf{s}_4 + \mathbf{s}_2 \mathbf{r}_{20}) \boldsymbol{\psi}_-, \quad (63)$$

from which we obtain

$$\mathbf{t}_{20} = (\mathbf{s}_4 + \mathbf{s}_2 \mathbf{r}_{20}). \quad (64)$$



Finally, in order to calculate the matrices  $\mathbf{t}_{02}$  and  $\mathbf{r}_{02}$ , we consider the reflection of light impinging at a semi-infinite anisotropic medium from vacuum. The electromagnetic field at the medium side is made up of two transmitted waves,  $\mathbf{F} = \sum_{\mu} \psi_{+}^{\mu} \mathbf{V}_{+}^{\mu} e^{ik_{\mu}z}$ . Imposing continuity on  $\mathbf{F}$  across the interface

$$\mathbf{F}_i + \mathbf{F}_r = \sum_{\mu} \psi_{+}^{\mu} \mathbf{V}_{+}^{\mu} e^{ik_{\mu}z}. \quad (65)$$

Writing the generalized vector field  $\mathbf{F}_i$  and  $\mathbf{F}_r$  in terms of the spinors  $\boldsymbol{\xi}_i = (\xi_i^p, \xi_i^s)^T$  and  $\boldsymbol{\xi}_r = (\xi_r^p, \xi_r^s)^T$  we get

$$\mathbf{F}_i = (\xi_i^p \cos \theta, \xi_i^p, \xi_i^s, \xi_i^s \cos \theta)^T \quad (66)$$

and

$$\mathbf{F}_r = (-\xi_r^p \cos \theta, \xi_r^p, \xi_r^s, -\xi_r^s \cos \theta)^T. \quad (67)$$

Substitution of this equation into Eq. (65) yields four linear algebraic equations that can be recast as two matrix equations for the spinors  $\boldsymbol{\psi}_{+}$ ,  $\boldsymbol{\xi}_i$  and  $\boldsymbol{\xi}_r$

$$\cos \theta (\boldsymbol{\xi}_i - \boldsymbol{\xi}_r) = \mathbf{s}_1 \boldsymbol{\psi}_{+} \quad (68)$$

and

$$\boldsymbol{\xi}_i + \boldsymbol{\xi}_r = \mathbf{s}_2 \boldsymbol{\psi}_{+}. \quad (69)$$

Elimination of  $\boldsymbol{\psi}_{+}$  from the last two equations yields

$$\boldsymbol{\xi}_r = \mathbf{r}_{02} \boldsymbol{\xi}_i, \quad (70)$$

where  $\mathbf{r}_{02}$  is given by Eq. (28). Elimination of  $\boldsymbol{\xi}_r$  from Eqs. (68)-(69) yields

$$\mathbf{t}_{02} = \mathbf{s}_1^{-1} \cos \theta (\mathbf{I} - \mathbf{r}_{02}). \quad (71)$$

This concludes the calculation of the reflection and transmission matrices corresponding to the front surface of the film.

- 
- [1] H. B. G. Casimir, Proc. Kon. Ned. Akad. Wet. **51**, 793 (1948).  
[2] P. W. Milonni, R. J. Cook, and M. E. Goggin, Phys. Rev. A **38**, 1621 (1988).  
[3] R. A. Beth, Phys. Rev. **50**, 115 (1936).  
[4] S. K. Lamoreaux, Phys. Rev. Lett. **78**, 5 (1997).  
[5] U. Mohideen, and A. Roy, Phys. Rev. Lett. **81**, 4549 (1998).  
[6] A. Roy, C. Y. Lin, and U. Mohideen, Phys. Rev. D **60**, 111101(R) (1999).  
[7] B. W. Harris, F. Chen, and U. Mohideen, Phys. Rev. A **62**, 052109 (2000).  
[8] M. Bordag, U. Mohideen, and V. M. Mostepanenko, Phys. Rep. **353**, 1 (2001).  
[9] F. Chen, U. Mohideen, G. L. Klimchitskaya, and V. M. Mostepanenko, Phys. Rev. A **66**, 032113 (2002).  
[10] F. Chen, U. Mohideen, G. L. Klimchitskaya, and V. M. Mostepanenko, Phys. Rev. A **73**, 019905 (2006).  
[11] H.B. Chan, V. A. Aksyuk, R. N. Kleinman, D. J. Bishop, and F. Capasso, Science **291**, 1941 (2001).  
[12] H. B. Chan, V. A. Aksyuk, R. N. Kleinman, D. J. Bishop, and F. Capasso, Phys. Rev. Lett. **87**, 211801 (2001).  
[13] D. Iannuzi, M. Lisanti, and F. Capasso, Proc. Natl. Acad. of Sci. (USA) **101**, 4019 (2004).  
[14] M. Lisanti, D. Iannuzi, and F. Capasso, Proc. Natl. Acad. of Sci. (USA) **102**, 11989 (2005).  
[15] G. Bressi, G. Carugno, R. Onofrio, and G. Ruoso, Phys. Rev. Lett. **88**, 041804 (2002).  
[16] R. S. Decca, E. Fischbach, G. L. Klimchitskaya, D.E. Krause, D. López, and V. M. Mostepanenko, Phys. Rev. D **68**, 116003 (2003).  
[17] R. S. Decca, D. López, E. Fischbach, G. L. Klimchitskaya, D. E. Krause, and V. M. Mostepanenko, Ann. of Phys. (N. Y.) **318**, 37 (2005).  
[18] E. M. Lifshitz, Sov. Phys. JETP **2**, 73 (1956).  
[19] V. A. Parsegian, and G. H. Weiss, J. Adhes. **3**, 259 (1972).  
[20] Y. S. Barash, Izv. Vyssh. Uchebn. Zaved., Radiofiz. **21**, 1637 (1978)[Radiophys. and Q. Elect. **12**, 1138 (1979)].  
[21] Y. S. Barash, and V. L. Ginzburg, Sov. Phys. Usp. **18**, 305 (1975).  
[22] D. Kupiszewska, Phys. Rev. A **46**, 2286 (1992).  
[23] S.J. van Enk, Phys. Rev. A **52**, 2569 (1995).

- [24] J. N. Munday, D. Iannuzzi, Y. Barash, and F. Capasso, Phys. Rev. A **71**, 042102 (2005).
- [25] C. G. Shao, A. H. Tong, and J. Luo, Phys. Rev. A **72**, 022102 (2005).
- [26] C. G. Shao, D. L. Zheng, and J. Luo, Phys. Rev. A **74**, 012103 (2006).
- [27] O. Kenneth, and S. Nussinov, Phys. Rev. D **63**, 121701(R) (2001).
- [28] H. Li, and M. Kardar, Phys. Rev. Lett. **67**, 3275 (1991).
- [29] H. Li, and M. Kardar, Phys. Rev. A **46**, 6490 (1992).
- [30] M. T. Jaekel, and S. Reynaud, J. Phys. **1**, 1395 (1991); C. Genet, A. Lambrecht, and S. Reynaud, Phys. Rev. A **67**, 043811 (2003).
- [31] A. Lambrecht, P. A. M. Neto, and S. Reynaud, New J. Phys. **8**, 243 (2006).
- [32] R. Esquivel-Sirvent, C. Villarreal, W. L. Mochán, and G. H. Cocoletzi, Phys. Status Solidi B **230**, 409 (2002).
- [33] W. L. Mochán, C. Villarreal, and R. Esquivel-Sirvent, Rev. Mex. Fís. **48**, 335 (2002).
- [34] R. Esquivel, C. Villarreal, and W. L. Mochán, Phys. Rev. A **68**, 052103 (2003).
- [35] R. Esquivel, C. Villarreal, and W. L. Mochán, Phys. Rev. A **71**, 029904 (2005).
- [36] W. L. Mochán, A. M. Contreras-Reyes, R. Esquivel-Sirvent and C. Villarreal, *Statistical Physics and Beyond: 2nd Mexican Meeting on Mathematical and Experimental Physics* ed. by F. J. Uribe *et al.* (AIP Conference Proceedings, vol 757) (American Institute of Physics, Melville, 2005) p 66.
- [37] P. Halevi, *Spatial Dispersion in Solids and Plasmas*, Electronic Waves Vol 1 (Amsterdam: North-Holland, 1992); P. Halevi, *Photonic Probes of Surfaces* (Amsterdam: Elsevier, 1995).
- [38] J. A. Stratton, *Electromagnetic Theory* (New York: Mc Graw-Hill, 1941).
- [39] P. A. M. Neto, A. Lambrecht, and S. Reynaud, Phys. Rev. A **72**, 012115 (2005).
- [40] R. B. Rodrigues, P. A. M. Neto, A. Lambrecht, and S. Reynaud, Phys. Rev. Lett. **96**, 100402 (2006).
- [41] R. B. Rodrigues, P. A. M. Neto, A. Lambrecht, and S. Reynaud, Europhys. Lett. **76**, 822 (2006).
- [42] F. S. S. Rosa, D. A. R. Dalvit, and P. W. Milonni Phys. Rev. A **78**, 032117 (2008).
- [43] R. Esquivel-Sirvent, C. Villarreal, and G. H. Cocoletzi, Phys. Rev. A **64**, 052108 (2001); C. Villarreal, R. Esquivel-Sirvent, and G. H. Cocoletzi, Int. J. of Modern Phys. A **17**, 798 (2002).
- [44] A. D. H. de la Luz, A. F. Alvarado-García, G. H. Cocoletzi *et al.*, Solid State Commun. **132**, 623 (2004).
- [45] R. Esquivel-Sirvent, C. Villarreal, W. L. Mochán, A. M. Contreras-Reyes, and V. B. Svetovoy, J. Phys. A: Math. Gen. **39**, 6323 (2006).
- [46] A. M. Contreras-Reyes, and W. L. Mochán, Phys. Rev. A **72**, 034102 (2005).
- [47] L. M. Procopio, C. Villarreal, and W. L. Mochán, J. Phys. A: Math. Gen. **39**, 6679 (2006).
- [48] J. C. Torres-Guzmán, and W. L. Mochán, J. Phys. A: Math. Gen. **39**, 6791 (2006).
- [49] W. L. Mochán, and C. Villarreal, New J. of Phys. **8**, 242 (2006).
- [50] T. P. Sosnowski, Opt. Commun. **4**, 408 (1972).
- [51] R. M. A. Azzam, N. M. Bashara, *Ellipsometry and polarized light* (Amsterdam:North-Holland, 1977).
- [52] G. B. Airy, Phil. Mag. **2**, 20 (1833).
- [53] D. W. Berreman, J. Opt. Soc. Am. **62**, 502 (1972).
- [54] M. Born, and E. Wolf, *Principles of Optics*, 7th. Edition (Cambridge University Press, 1999).
- [55] F. Intravia, and A. Lambrecht, Phys. Rev. Lett. **94**, 110404 (2005).
- [56] L. Bergstrom, Adv. Colloid Interface Sci. **70**, 125 (1997).
- [57] Jeremy N. Munday, Davide iannuzzi, and Federico Capasso, New J. Phys. **8**, 244 (2006).